# Origin of High Mountains in the Continents: The Southern Sierra Nevada

Brian Wernicke,* Robert Clayton, Mihai Ducea, Craig H. Jones, Stephen Park, Stan Ruppert, Jason Saleeby, J. Kent Snow, Livia Squires, Moritz Fliedner, George Jiracek, Randy Keller, Simon Klemperer, James Luetgert, Peter Malin, Kate Miller, Walter Mooney, Howard Oliver, Robert Phinney

Active and passive seismic experiments show that the southern Sierra, despite standing 1.8 to 2.8 kilometers above its surroundings, is underlain by crust of similar seismic thickness, about 30 to 40 kilometers. Thermobarometry of xenolith suites and magnetotelluric profiles indicate that the upper mantle is eclogitic to depths of 60 kilometers beneath the western and central parts of the range, but little subcrustal lithosphere is present beneath the eastern High Sierra and adjacent Basin and Range. These and other data imply the crust of both the High Sierra and Basin and Range thinned by a factor of 2 since 20 million years ago, at odds with purported late Cenozoic regional uplift of some 2 kilometers.

What holds up high mountain belts on continents? The Earth's two highest belts, the Himalaya-Tibet collision zone and the central Andes, are supported by Airy-type crustal roots 70 to 80 km thick, almost twice that of adjacent lowlands (*1*). A 30- to 35-km increase in crustal thickness should raise elevation by about 4500 m, in agreement with observed differences in elevation in these two cases (*3*). The Sierra Nevada, one of the major mountain ranges in North America, lies at an elevation of 2800 m but is enigmatic. It contains the highest point in the lower 48 states (Mount Whitney, 4419 m), yet just a short distance away, Death Valley lies below sea level, within a zone of strong crustal extension (*4*). In addition, conflicting seismic interpretations have been presented as to whether the High Sierra (roughly the eastern third of the range) is underlain by a crust 55 km thick (*5*) or by crust only 30 to 40 km thick (*6*), similar to that of surrounding lowlands of the Basin and Range and Great Valley (Fig. 1).

We collected wide-angle refraction-reflection data along profiles transverse to (east-west) and parallel to (north-south) the structural grain (Fig. 1). The question of a crustal root is most clearly addressed by the seismic sections from shot point 5, just east of the High Sierra, and shot point 24, near the east end of the line (Fig. 1). As shown in Fig. 2A, the *PmP* (Moho reflection) phase is evident on stations both to the east and west of the source point. Stations to the west record *PmP* reflections from directly beneath the Sierra whereas recordings to the east are for reflection points beneath the Basin and Range. Travel times for the western branch are only ~0.5 s greater than the corresponding times for the eastern branch. Apparent *Pg* (upper crustal) phase velocities across the Sierra varied by <0.2 km/s. For a laterally invariant mean crustal velocity of 6.3 km/s, the *PmP* delays to the west allow a crustal root of only 3 to 4 km. The absence of a large crustal root is also clear from $P_n$ (Moho refraction) recordings from shot point 24. These do not show a major delay or decrease in amplitude when passing under the Sierra Nevada (Fig. 2B).

The absence of a large crustal root is also suggested by teleseismic *P* to *S* (*Ps*) mode conversions from the Moho observed at three passive seismic arrays on the east-west refraction line. Beam-formed seismograms (*7*) penetrating the Moho between arrays in the central and eastern Sierra have a *Ps* arrival about 4.2 s after the *P*. For an average *P* velocity of 6.2 ± 0.2 km/s and Poisson's ratio of 0.25 ± 0.04 for the crust, the *Ps* arrivals indicate that the Moho is 33 ± 5 km below sea level. Similar measurements for an array in the Basin and Range 40 km east of shot point 5 indicate that the Moho is also ~33 km below sea level.

Our structural model of the data (Fig. 3A) incorporates lateral velocity changes in the top 15 km, but these variations are incapable of supporting the topography. The *Pg* and $P_n$ travel time observations only permit lateral variations in mean crustal *P* velocities of about 3%, equivalent to lateral density variations of about 2% for Nafe-Drake or Birch velocity-density relations (*8*). Such variations would only accommodate elevation differences of ~500 to 600 m, less than 25% of that observed. Even allowing for large, systematic deviations from commonly used velocity-density relations, at most half of the Sierran topography and gravity signature can be ascribed to lateral density variations in the crust (Fig. 3B). The topography, gravity, and crustal structure of the southern Sierra Nevada thus provide an example of a continental mountain range supported mainly by lateral density variations in the upper mantle, or a Pratt-type root.

We modeled support of Sierran topography through a combination of lateral variations of density in the crust (~25% of the effect, including that of a small crustal root) and in the mantle (~75%). Such a combination explains the main anomalies in the gravity field (Fig. 3B). Variations in *Ps* conversion amplitudes recorded by the passive arrays might reflect this upper mantle anomaly, as *Ps* amplitudes are smaller under



B. Wernicke, R. Clayton, M. Ducea, J. Saleeby, J. K. Snow, L. Squires, Division of Geological and Planetary Sciences 170-25, California Institute of Technology, Pasadena, CA 91125, USA.
C. H. Jones, CIRES, University of Colorado, Boulder, CO 80309, USA.
S. Park, Department of Earth Sciences, University of California, Riverside, CA 92521, USA.
S. Ruppert, Lawrence Livermore National Laboratory, Livermore, CA 94550, USA.
M. Fliedner and S. Klemperer, Department of Geophysics, Stanford University, Stanford, CA 94305, USA.
G. Jiracek, Department of Geological Sciences, San Diego State University, San Diego, CA 92182, USA.
R. Keller and K. Miller, Department of Geological Sciences, University of Texas, El Paso, TX 79968, USA.
J. Luetgert, W. Mooney, H. Oliver, U.S. Geological Survey, Menlo Park, CA 94025, USA.
P. Malin, Department of Geology, Duke University, Durham, NC 27708, USA.
R. Phinney, Department of Geological and Geophysical Sciences, Princeton University, Princeton, NJ 08544, USA.
*To whom correspondence should be addressed.

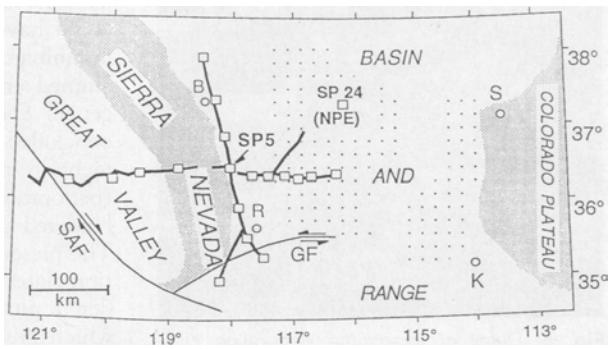


**Fig. 1.** Distribution of receivers for wide-angle reflection/refraction experiment (heavy lines) and shot points (squares) relative to the southern Sierra Nevada and environs. The northwest-trending segment projecting toward shot point (SP) 24 corresponds to the receiver array along the east end of the east-west profile in Fig. 2B. Open circles correspond to the following cities: B, Bishop; K, Kingman; R, Ridgecrest; S, Saint George. Thin lines with arrows show major strike-slip faults and senses of slip; GF, Garlock fault; SAF, San Andreas fault. Dotted areas are zones of strong upper crustal extension (>300%) within the Basin and Range province (*4*).

the High Sierra than elsewhere and are followed by additional conversions between 7 and 9 s after *P*. Incorporation of such an upper mantle anomaly would only visibly affect seismic arrivals near the Sierra. Reduction of $P_n$ velocities under the High Sierra by 2 to 5% improves our fit to $P_n$ arrival times, confirming previously inferred low $P_n$ velocities from both north-south (6) and east-west (*11*) profiles. The absence of low $P_n$ velocities outside the High Sierra region corroborates higher $P_n$ values from previous work to the west [for example, (*12*)] and east (6, *13*).

The position of an upper mantle seismic anomaly under the High Sierra is also suggested by an electrical conductivity anomaly and by variations in mantle xenolith suites. Magnetotelluric (MT) data at 30 stations along the seismic line indicate several zones of enhanced conductivity in the lower crust and upper mantle (Fig. 4A).

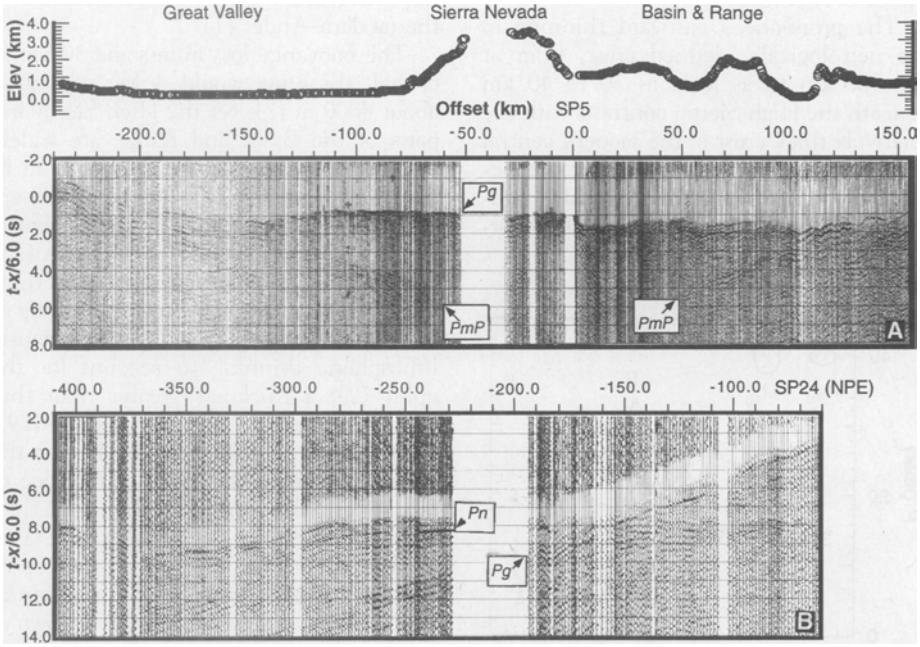


**Fig. 2.** East-west seismic profiles across the southern Sierra Nevada showing *Pg*, $P_n$, and *PmP* phases; (**A**) from shot point 5 (Fig. 1); upper panel shows horizontal position and elevation of receivers; (**B**) from shot point 24 (nonproliferation explosion or NPE); receiver locations are approximately the same as those in (A), except east of offset −135 km receivers lie along the northwest line projecting toward the shot point (Fig. 1). Note that variations in receiver elevation and basin fill may cause small perturbations in arrival times (<0.5 s). The delays of 1 to 2 s beneath the Great Valley in (B) are mainly due to thick Cenozoic sediments.

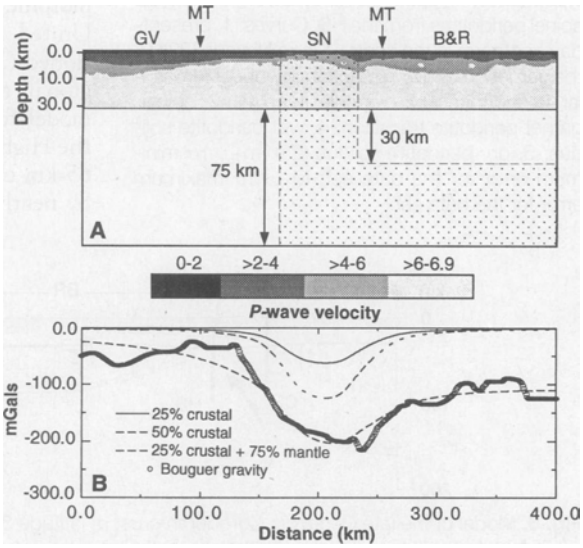


**Fig. 3.** (**A**) East-west structural model inferred from seismic data. The top 10 to 15 km is taken from a tomographic analysis (*9*) and primarily reflects the static time delays introduced by the sediment-filled basins. The mid to lower part of the model was verified by finite-difference modeling of the east-west shot points. The positioning of the Moho at a depth of 33 km is based on *Ps* conversions; the depth may be greater than 40 km in some areas, especially north of 37°N (*10*). Arrows show boundaries of MT profile in Fig. 4A. (**B**) Bouguer gravity and gravity models computed by varying crustal density within stippled area proportionally with topography. Upper two models show effect of average crustal density contrasts of 50 and 100 kg/m$^3$ (within local variation proportional to topography), corresponding to 25 and 50% of the total compensation needed, respectively. Lower model curve shows a 25% crustal contribution and 75% mantle contribution, assuming stippled region in the upper mantle is 80 kg/m$^3$ less dense than unpatterned area.

The most striking features of the model are localized regions of low resistivity beneath the western Sierra and Great Valley; these may be explained by conductive metasedimentary rocks. A broad zone of lower resistivity is evident in the upper mantle beneath the eastern Sierra. The data imply that mean upper mantle resistivity is between 3 and 30 ohm·m, with a preferred value of 10 to 20 ohm·m (Fig. 4B). The cause of such low resistivities is likely partial melt because of the absence of conductive solid phases in the mantle and because saline fluids cannot maintain interconnected networks in ultramafic rocks at these pressures and temperatures (*16*). Partial melt fractions of 1.5 to 16% can explain the range of resistivities in the upper mantle (*17*), but melt fractions of 2 to 5% best fit the data. For magma density of 2740 kg/m$^3$, 5% partial melt reduces the bulk density of mantle by only 25 kg/m$^3$. Upper mantle heated to subsolidus temperatures has a density about 50 kg/m$^3$ less than cooler mantle. The MT data thus suggest a density decrease of about 75 kg/m$^3$ (~2.4%) distributed beneath the eastern Sierra Nevada from depths of 35 to 80 km (Fig. 3B).

Xenoliths from Late Cenozoic volcanic flows from the central Sierra (CS suite), the High Sierra, Owens Valley, and Inyo Mountains (HS suite) show variations in texture, composition, and thermal history consistent with the MT and seismic anomalies. The CS suite includes feldspathic granulites, garnet-pyroxenites, eclogites, cumulate gabbros and amphibolites, garnet and spinel peridotites, and garnet websterites (*18*–*20*). The HS suite includes spinel lherzolites, harzburgites, spinel dunites, spinel websterites, clinopyroxenites, gabbros, and mafic granulites, but lacks garnet. Melt inclusions are common in the HS xenoliths, with an average of 2 to 3% in thin sections.

The HS xenoliths record much higher temperatures than does the CS suite. In the CS suite, the lower crustal feldspathic granulites and the garnet clinopyroxenites are likely batholith-related rocks. The thermobarometric data (Trend A, Fig. 5) imply that deeper rocks cooled more slowly and equilibrated at lower temperatures than did the shallower rocks. The deepest crustal xenoliths are from ~60 km, within the seismically defined upper mantle. The basalt-eclogite phase transition occurs at ~35 km for the recorded temperatures (similar to the depth of seismic Moho), and the thermobarometric measurements are consistent with the basalt-eclogite transition predicted by the mineral compositions of the CS xenoliths. These results suggest that the Moho is at least 25 km shallower than the compositional boundary between mafic and ultramafic rocks. Pressure-temperature

data for CS garnet peridotites and garnet websterites (*19*) yield an adiabatic slope (Trend B, Fig. 5), suggesting that the convective upper mantle was as shallow as ~60 km. The HS xenoliths also define an adiabatic slope (Trend C, Fig. 5), but to depths of only 30 to 40 km, and are ~250°C hotter than for the CS suite.

The high topography, thin crust, low $P_n$ velocity, enhanced upper mantle conductivity, and shallow, hot, melt-bearing upper mantle xenoliths collectively suggest that the asthenospheric upper mantle lies near the depth of the Moho beneath the High Sierra, whereas the upper mantle to the west contains a thick, relatively cold eclogitic root. During the Mesozoic, under the high heat flow conditions of an active magmatic arc, the Moho would have been much deeper because of depression of the gabbro-eclogite phase transition, so the crustal thickness in the central Sierra would likely have been ~60 km or more. The strong contrast in present-day mantle heat flux across the range, which is low in the west and high in the east (*22*), may suggest that the High Sierran mantle lithosphere has thinned recently, perhaps related to Neogene crustal extension in the Basin and Range (*24*) (Fig. 6).

The pronounced eastward thinning of the petrologically defined crust, from at least 60 km to as little as 30 to 40 km beneath the High Sierra, contrasts with the relatively thick crust of the modern central Andes (*1*), generally considered a close tectonic analog for the pre-extensional Cordillera (*25*). The High Sierra has similar crustal structure to that of the adjacent Basin and Range, where the upper crust has been tectonically extended some 250 to 300 km in a west-northwest direction over the last 15 to 20 million years (Fig. 6) (*26*). Reconstruction of the extension yields an overall thinning of the crust by about a factor of 2, for an initial crustal thickness of 60 to 70 km, depending on the volume of magma added during extension. This would be roughly consistent with the thick petrologically defined crust in the western and central Sierra, and with the crustal thickness of the modern Andes (*1*).

The buoyancy loss from some 30 km of crustal thinning would lower elevation about 4000 m (*2*), yet the High Sierra and parts of the Basin and Range are widely believed to have risen 1500 to 2000 m in the late Cenozoic (*27*). An extraordinary contribution to buoyancy from the mantle, which not only accounts for the uplift (*28*) but counteracts the effect of crustal thinning, would be needed. Crustal thinning of 30 km would require over 200 km of mantle lithospheric thinning to account for the uplift (*2*), a thickness greater than that estimated even for Archean cratons (*29*). One solution to this difficulty is that the density change in the upper mantle due to lithospheric thinning is much greater than commonly assumed, perhaps in part as a result of a compositional effect, such as Fe depletion of the upper mantle from partial melting (*30*) or metamorphic breakdown of garnet in the upper mantle due to heating from magmatism and extension to the east. The absence of garnetiferous samples in eastern Sierran xenoliths versus the garnet-rich rocks to the west may support this hypothesis. Alternatively, the Sierra may have maintained or even lost elevation in the late Cenozoic, as paleofloral and geomorphic arguments for uplift of the western United States have recently been questioned (*31*). Allowing the possibility of regional topographic lowering, a plausible model for the late Cenozoic evolution of the High Sierra might include thinning of a 65-km crust down to 35 km, accompanied by nearly complete removal of a relatively

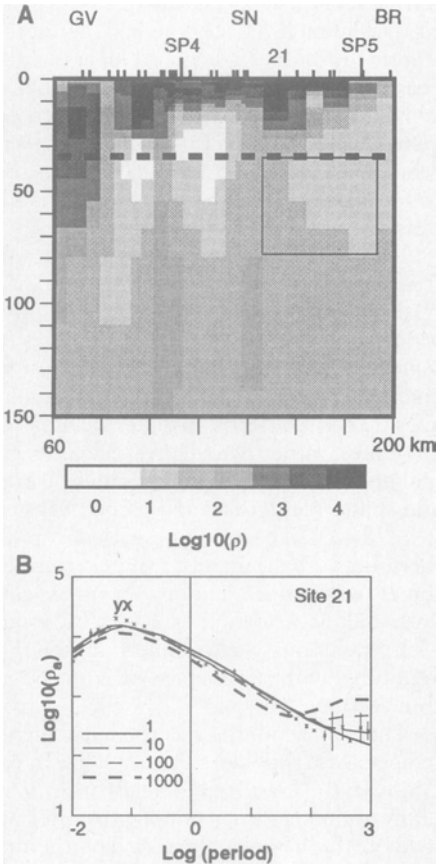


**Fig. 4.** (**A**) East-west resistivity model resulting from inversion of distortion-corrected MT data for minimum structure model (*14, 15*). Vertical scale in kilometers; horizontal scale corresponds to model coordinates of Fig. 3, showing position of shot point 5 (SP5) and MT site 21. GV, Great Valley; SN, Sierra Nevada; BR, Basin and Range. Box in upper mantle beneath the eastern Sierra Nevada outlines region perturbed for sensitivity tests in (B). (**B**) Sensitivity of MT sounding at site 21 in the Sierra Nevada to upper mantle conductivity. Apparent resistivities for the *yx* mode (perpendicular to geologic strike) show variations due to perturbation of upper mantle resistivities from 1 to 1000 ohm·m. Trial values of upper mantle resistivity are in the box in (A). Values of 3 to 30 ohm·m for upper mantle resistivity provide acceptable fits.

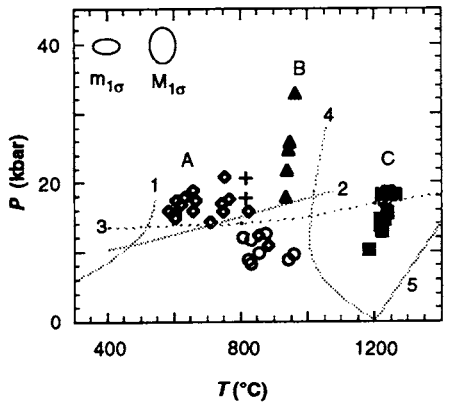


**Fig. 5.** Equilibration pressure-temperature determinations on Sierra Nevada xenoliths (*19, 21*). Trends A, B, and C are explained in the text. Symbols: ○, feldspathic granulites; ◇, garnet clinopyroxene rocks; ▲, garnet peridotites and garnet websterites; +, spinel peridotites from the CS; ■, spinel peridotites from the HS. Curves: 1, present-day geotherm in the central Sierra Nevada (*22*); 2, the garnet breakdown reaction: pyrope + grossular = anorthite + 2 diopside + spinel; 3, spinel-garnet peridotite transition; 4, wet peridotite solidus; 5, dry peridotite solidus (*23*). $m_{1\sigma}$, $1\sigma$ minimum error for the data set; $M_{1\sigma}$, $1\sigma$ maximum error for the data set.

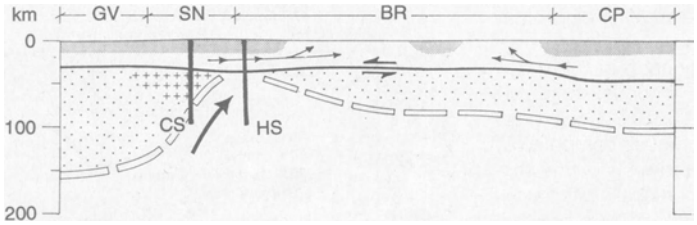


**Fig. 6.** Model of the late Cenozoic Cordilleran crust at latitude 36.5°N. Shading, pre-20 million-year-old upper crust; unpatterned layer with flow lines, fluid deep crust; +, eclogitic upper mantle; dots, mantle lithosphere; dashed line, 1000°C isotherm; bold arrow, locus of asthenospheric upwelling below the High Sierra; GV, Great Valley; SN, Sierra Nevada; BR, Basin and Range; CP, Colorado Plateau; CS, column of central Sierran xenolith suite; HS, column of High Sierra–Owens Valley xenolith suite.

cold, 70- to 80-km-thick mantle lid (Fig. 6). This would suggest a history where the range lay at about 4000 to 5500 m, and then subsided to 2000 to 3000 m as a result of extension (32).

## REFERENCES AND NOTES


1. W. J. Zhao *et al.*, *Nature* **366**, 557 (1993); G. Zandt, A. A. Velasco, S. L. Beck, *Geology* **22**, 1003 (1994).
2. Assuming isostatic equilibrium, a change $\Delta h$ in the thickness of any given layer in the lithosphere results in elevation change $\Delta e = \Delta h\,(\rho_a - \rho_e)/\rho_a$ where $\rho_e$ is the density of the layer. Here we assume that $\rho_a$ = 3250 kg/m$^3$ and the average density of the crust is 2800 kg/m$^3$.
3. *The New York Times Atlas of the World* (Random House, New York, ed. 4, 1994); in this paper, elevation refers to regionally averaged elevations [for example, W. H. Diment and T. C. Urban, *U.S. Geol. Surv. Geophys. Invest. Map, GP-933* (1981)], which may be considered isostatically compensated.
4. B. Wernicke, in *The Geology of North America*, B. C. Burchfiel, P. W. Lipman, M. L. Zoback, Eds. (The Geological Society of America, Boulder, CO, 1992), vol. G-3, chap. 12.
5. J. P. Eaton, *Calif. Div. Mines Geol. Bull.* **190**, 419 (1966); L. C. Pakiser and J. N. Brune, *Science* **210**, 1088 (1980); W. D. Mooney and C. S. Weaver, *Geol. Soc. Am. Mem.* **172**, 129 (1989); *P*-wave velocity of the root was suggested to be 6.9 km/s.
6. C. H. Jones, H. Kanamori, S. W. Roecker, *J. Geophys. Res.* **99**, 4567 (1994).
7. Arrays combine three broad-band (10- or 30-s period) and six to eight short-period seismometers in an L-shaped or linear array. Traces are summed into beams using a time-shift so that the teleseismic *P* arrives simultaneously on all traces, thus greatly reducing scattered and reflected energy.
8. F. Birch, *J. Geophys. Res.* **66**, 2199 (1961); W. J. Ludwig, J. E. Nafe, C. L. Drake, in *The Sea: Ideas and Observations on Progress in the Study of the Seas*, A. E. Maxwell, Ed. (Wiley Interscience, New York, 1970), vol. 4, pp. 53–84.
9. S. Ruppert and M. M. Fliedner, unpublished data.
10. Variations in *PmP* arrival times for the north-south profile indicate only a 2° northward dip on the Moho, consistent with analysis of fan shots (M. M. Fliedner and S. Ruppert, unpublished data), justifying neglect of three-dimensional effects for the purposes of this analysis.
11. D. S. Carder, *Bull. Seismol. Soc. Am.* **63**, 571 (1973).
12. D. H. Oppenheimer and J. P. Eaton, *J. Geophys. Res.* **89**, 10,267 (1984); W. S. Holbrook and W. D. Mooney, *Tectonophysics* **140**, 49 (1987).
13. J. F. Gibbs and J. C. Roller, *U. S. Geol. Surv. Prof. Pap. 550-D* (1966), p. D125.
14. R. W. Groom and R. C. Bailey, *J. Geophys. Res.* **94**, 1913 (1989); J. T. Smith and J. R. Booker, *ibid.* **96**, 3905 (1991).
15. S. K. Park, B. Kirasuna, G. Jiracek, C. Smith, unpublished data.
16. E. B. Watson and J. M. Brenan, *Earth Planet. Sci. Lett.* **85**, 497 (1987).
17. T. J. Shankland, R. J. O'Connell, H. S. Waff, *Rev. Geophys. Space Phys.* **19**, 394 (1981).
18. F. C. Dodge, L. C. Calk, R. W. Kistler, *J. Petrol.* **27**, 1277 (1986).
19. F. C. Dodge, J. P. Lockwood, L. C. Calk, *Geol. Soc. Am. Bull.* **100**, 938 (1988); B. Mukhopadhyay, thesis, University of Texas at Dallas (1989); B. Mukhopadhyay and W. I. Manton, *J. Petrol.* **35**, 1417 (1994).
20. Trace element investigations (M. N. Ducea, R. W. Kistler, J. B. Saleeby, unpublished data) rule out any link with the host volcanic rocks.
21. Mineral rim compositions of 31 CS and HS samples displaying textural equilibrium were determined using the Caltech JEOL 733 electron microprobe. Geobarometers used included net-transfer reactions such as Al-in-orthopyroxene co-existing with garnet [S. L. Harley and D. H. Green, *Nature* **300**, 697 (1984)], while geothermometers involved mainly Fe-Mg exchange reactions [for example, R. Powell, *J. Metamorphic Geol.* **3**, 231 (1985)].
22. A. H. Lachenbruch, *J. Geophys. Res.* **73**, 6977 (1968); R. W. Saltus and A. H. Lachenbruch, *Tectonics* **10**, 325 (1991).
23. Basaltic Volcanism Study Project, *Basaltic Volcanism in the Terrestrial Planets* (Pergamon, New York, 1981).
24. B. Wernicke, *Can. J. Earth Sci.* **22**, 108 (1985); C. H. Jones, *Tectonics* **6**, 449 (1987); C. H. Jones *et al.*, *Tectonophysics* **213**, 57 (1992).
25. B. C. Burchfiel, D. S. Cowan, G. A. Davis, in *The Geology of North America*, B. C. Burchfiel, P. W. Lipman, M. L. Zoback, Eds. (The Geological Society of America, Boulder, CO, 1992), vol. G-3, chap. 8.
26. Two domains of extreme upper crustal extension (>300%) are interspersed with little-extended areas (<10 to 15%) that include parts of the Basin and Range, Sierra Nevada, and Colorado Plateau [Fig. 1; B. Wernicke, G. J. Axen, J. K. Snow, *Geol. Soc. Am. Bull.* **100**, 1738 (1988)]. Downward extrapolation of extension through the entire crust results in an improbable reconstruction, with 90- to 100-km-thick crust interposed with areas of 35-km-thick crust. Fluid behavior of the deep crust across the region, such that it is hydraulically pumped toward areas of upper crustal extension [for example, B. Wernicke, in *Exposed Cross Sections of the Continental Crust*, M. Salisbury and D. Fountain, Eds. (Kluwer, Dordrecht, Netherlands, 1990), pp. 509–544] results in a relatively flat reconstructed Moho (Fig. 6).
27. M. N. Christensen, *Geol. Soc. Am. Bull.* **76**, 1105 (1966); J. R. Unruh, *ibid.* **103**, 1395 (1991); N. K. Huber, *U. S. Geol. Survey Prof. Pap. 1197* (1981); D. I. Axelrod, *Univ. Calif. Publ. Geol. Sci.* **121** (1980); T. A. Dumitru, *J. Geophys. Res.* **95**, 4925 (1990).
28. S. T. Crough and G. A. Thompson, *Geology* **5**, 396 (1977); G. A. Thompson and M. L. Zoback, *Tectonophysics* **61**, 149 (1979).
29. J. Polet and D. L. Anderson, *Geology* **23**, 205 (1995).
30. S. I. Akimoto, *Tectonophysics* **13**, 167 (1972); T. H. Jordan, in *The Mantle Sample*, F. R. Boyd and H. O. A. Meyer, Eds. (American Geophysical Union, Washington, DC, 1979), vol. 2, pp. 1–14.
31. C. E. Forest, P. Molnar, K. A. Emanuel, *Nature* **374**, 347 (1995); E. E. Small and R. S. Anderson, *Science* **270**, 277 (1995).
32. We assume that the mean crustal density is 2700 to 2800 kg/m$^3$ and use calculations of A. H. Lachenbruch and P. M. Morgan [*Tectonophysics* **174**, 39 (1990)].


33. Supported by the Continental Dynamics Program of the National Science Foundation (EAR-9120690 to S.P., EAR-9120688 to G.J., EAR-9119263 to P.M., and EAR-9120689 to R.P.), the Department of Energy (DE-FG03-93ER14311 to R.C.), the U.S. Navy (China Lake Naval Weapons Center), and the U.S. Air Force (Office of Scientific Research). Key logistical support was provided by the National Park Service, Bureau of Land Management, and U.S. Forest Service.

30 August 1995; accepted 14 November 1995


# Fluorination of Diamond Surfaces by Irradiation of Perfluorinated Alkyl Iodides


V. S. Smentkowski and John T. Yates Jr.*



**A facile method for chemically functionalizing diamond surfaces has been developed using x-ray irradiation of perfluoroalkyl iodide layers on the surface. Perfluoroalkyl radicals chemically bond to the diamond surface and can be thermally decomposed to produce strongly bound surface C–F bonds that are stable at high temperatures.**


Diamond film coatings can significantly improve the surface properties of many materials in applications such as cutting tools, biological implants, optical disks, lenses, and windows (*1*). In each of these applications, it may be desirable to modify the properties of the outer surface of the diamond film itself to produce special surface properties. The chemical modification of diamond surfaces is one route for producing useful surface properties. One modifier that offers promise for the improvement of the behavior of diamond surfaces is fluorine (*2*); the strong C–F bonds of fluorine (*3*) on diamond surfaces provide enhanced lubricity (*4*) and enhanced stability under oxidizing conditions at elevated temperatures (*5*).

Until now, diamond surfaces have been fluorinated only with extreme methods involving molecular $F_2$ (*5*), atomic F (*6*), $XeF_2$ (*4*, *7*), and fluorine-containing plasmas (*8*). Each of these surface-modification methods involves the handling of corrosive gases under harsh treatment conditions. In addition, only partial fluorination of the diamond surfaces studied was achieved with these extreme methods (*4*–*8*). A recent, extensive review showed that the attachment of long chain fluoroalkyl species directly to diamond surfaces has not been reported (*9*), although attachment of such species by silylation on oxidized diamond is known (*10*).

We present a method for the deposition of more than one F atom per surface C atom on diamond. The fluorinated alkyl layer achieved by this method decomposes between 300 and 700 K to produce a highly stable form of chemisorbed fluorine on the diamond surface that then thermally decomposes over a wide temperature range up to 1500 K (*11*).

Perfluorinated alkyl iodides ($C_xF_{2x+1}I$) were used as a source of radiation-produced perfluorinated alkyl radicals that attack the diamond surface and anchor themselves there. Irradiation with x-rays dissociated the weak C–I bond (*3*, *12*) in both $C_4F_9I$ and $CF_3I$ layers condensed on a diamond (100) single crystal (*11*). The x-ray irradiation was used also for x-ray photoelectron spectroscopy (XPS) measurements of the nature of the surface layer. The diamond


Surface Science Center, Department of Chemistry, University of Pittsburgh, Pittsburgh, PA 15260, USA.

*To whom correspondence should be addressed.